Research Article

Research on Underwater Sound Source Localization Based on NLM-EEMD and FCM-Generalized Quadratic Correlation

Shizhe Wang, Zongji Li, Pingbo Wang, and Yuchen Sun

Naval University of Engineering, Wuhan 430033, China

Correspondence should be addressed to Pingbo Wang; 1594984655@qq.com

The accuracy of underwater sound source localization depends on the preprocessing effect of signal denoising and delay estimation performance. In order to meet the needs of high-precision underwater positioning, this article studies a time delay estimation method based on nonlocal mean-enforced mean empirical mode decomposition (NLM-EEMD) autocorrelation denoising preprocessing and fuzzy C-means clustering (FCM)-generalized quadratic for underwater sound source localization technology. The theories such as NLM, EEMD, FCM, and generalized quadratic correlation delay estimation are studied in detail, and the speech signal of the test library in the TIMIT standard library is selected for simulation analysis, which verifies the correctness of the delay estimation method. Experiments were carried out in a larger outdoor pool. The analysis results show that the NLM-EEMD adaptive denoising method effectively reduces noise interference and improves the quality of EEMD decomposition and the FCM-generalized quadratic correlation method increases the correlation between two signals. The time delay estimation accuracy is improved, and the positioning accuracy is 48.66% higher than that of the direct generalized cross-correlation method.

1. Introduction

Underwater sound source localization has always been the focus and hot issue of hydroacoustic research and is widely used in military and civil fields such as ocean exploration and development, coastal defense, etc. Sound source localization techniques based on acoustic sensor arrays can be divided into three categories: localization methods based on maximum controllable response power beamforming, localization methods based on high-resolution spectral estimation, and localization methods based on TDOA. Carter first proposed the sound source location method of maximum controllable response power beamforming in 1977 [1] and later generations continue to optimize and improve it. Dibiase Joseph Hector proposed the SPR-PHAT method [2]; Wan and Wu proposed the SRP method [3] based on the principal eigenvector; and Do and Silverman and Lima et al. proposed an improved search method from coarse to fine, which greatly reduced the amount of computation [4, 5]. However, this location method requires a priori knowledge of the sound source and environmental noise, it is sensitive to the initial search value, and it not only reduces the amount of calculation but also reduces the accuracy of estimation [6]. The spatial resolution of the positioning method based on high-resolution spectral estimation is not limited by the signal sampling frequency, and arbitrary positioning accuracy can be achieved under certain conditions. However, this method relies on searching the entire space to determine the location of the sound source, which is more expensive and complex than other algorithms [7, 8]. This method is generally not used in single sound source positioning. Compared with the first two methods, the positioning technology based on TDOA is the simplest one, with high positioning accuracy, less computation, and good real-time performance. It can achieve good results in the application of single sound source positioning [9].

Time delay estimation accuracy is the decisive factor to determine TDOA positioning accuracy. Preprocessing underwater acoustic signals such as denoising or optimizing time delay estimation algorithms are effective methods to

improve time delay estimation accuracy and target positioning accuracy. Knapp et al. and Mosayyebpour et al. estimate time delay based on generalized cross-correlation, cross power spectrum phase, quadratic correlation, adaptive least mean square (LMS), acoustic transfer function, subspace decomposition, and cepstrum filtering methods [10–16]. Jiafan Yin and Lu Yang et al. used the NLM method to denoise the human ECG signal and eddy current sensor signal, respectively [17, 18]. Lu, Liu, and Zhang et al. used the EEMD method to denoise the microseismic signal, pulse signal, and blasting vibration signal of underground mines, respectively [19–21]. Li, Yu, and Su et al. combined the FCM method to process pipeline leakage signal, EEG signal, and micro-Doppler radar intermediate frequency signal, respectively [22–24].

Based on the above research, this article proposes an underwater sound source location method based on NLM-EEMD and FCM-generalized quadratic correlation. First, NLM-EEMD autocorrelation denoising is performed on the collected signal, which makes up for the unsatisfactory denoising effect of EEMD on low SNR signals. Then FCM fuzzy clustering is performed to adaptively extract the effective segment of the signal, making the correlation peak after generalized quadratic correlation time delay estimation more prominent; thus, the accuracy of sound source location is improved [22].

2. NLM-EEMD Signal Denoising Algorithm

2.1. NLM Algorithm.
Let the signal model be expressed as $y(t) = x(t) + n(t)$, where $y(t)$ is the sound sensor that actually collects signals, $x(t)$ is valid signal, and $n(t)$ is noise signal.

For one-dimensional signals $y(t)$, denoising processing [18, 25–30] based on NLM is to eliminate the interference of noise $n(t)$, it is the process of recovering valid signal $x(t)$, and is the weighted average of finding all similar blocks in the entire search area $M(t)$ [31, 32], the weighted mean $K(t)$ can be obtained by

$$K(t) = \frac{1}{Z(t)} \sum_{s \in M(t)} \omega(t,s) y(t), \tag{1}$$

where $Z(t)$ represents the sum of the similarity degrees of all similar blocks, that is, the normalization factor, and the calculation equation is as follows:

$$Z(t) = \sum_{s \in M(t)} \omega(t,s), \tag{2}$$

where $\omega(t,s)$ is the weight, and the calculation equation is as follows:

$$\omega(t,s) = e^{-\dfrac{\sum_{\delta \in \Delta} (y(t+\delta) - v(s+\delta))^2}{h^2}} = e^{\dfrac{-d^2(s,t)}{2L_\Delta \lambda^2}}, \tag{3}$$

where d^2 represents the sum of the squares of the Euclidean distance of the neighborhood blocks of the two sample points t and s, h controls the decay speed of $\omega(t,s)$, the value is $h = \lambda \sqrt{2L_\Delta}$, Δ represents the neighborhood block centered on the t sample point, L_Δ represents the neighborhood block

centered on the s sample point, λ represents the bandwidth parameter, and its value is expressed as $\lambda = 0.5\sigma$ according to the SURE criterion, where σ is the signal variance.

The weight $\omega(t,s)$ depends on the similarity between the sample points s and t and satisfies the following conditions:

$$\begin{cases} \dfrac{0 \leq \omega(t,s)}{Z(t) \leq 1} \\ \dfrac{\sum_j \omega(t,s)}{Z(t) = 1} \end{cases}. \tag{4}$$

The parameter relationship diagram of the NLM algorithm is shown in Figure 1. N represents half of the search area M, and the parameters P, λ, and N jointly determine the final result of the filtering.

2.2. EEMD Algorithm.
Empirical mode decomposition (EMD) is essentially a method of decomposing the time domain signal according to the frequency domain scale, producing a series of intrinsic mode function (IMF) components with different characteristics and a residual component; it is different from variational modal decomposition (VMD) [33, 34]. But EMD decomposition may cause modal aliasing problems and endpoint effects, so the EEMD decomposition method has been developed. The steps of the EEMD algorithm [21, 22] are as follows [35–39]:

(1) Gaussian white noise is added to the target signal:

$$x_i(t) = x(t) + n_i(t), i = 1, 2, \cdots, N. \tag{5}$$

(2) The noise-added signal $x_i(t)$ is decomposed by EMD to obtain multiple groups of IMF components IMF_k^i, where $k = 1, 2, \cdots, K$, K is the decomposition scale.

(3) The average value of each group of IMF components is calculated as the final value of EEMD decomposition:

$$IMF_k = \frac{1}{N} \sum_{i=1}^{N} IMF_k^i, k = 1, 2, \cdots, K. \tag{6}$$

The screening process of EEMD is adaptive. In the decomposition process, the Gaussian white noise signal is added, and the Gaussian white noise can be used to cancel each other when multiple trials are superimposed, and the abnormal events in the original signal are "smoothed." Therefore, it is a noise-assisted data analysis method, which solves the modal aliasing problem that may occur in EMD and makes the denoising effect better and the final sound source localization accuracy higher. The EEMD decomposition flow chart is shown in Figure 2.

2.3. Combination of NLM and EEMD to Reduce Noise.
The signal is first preprocessed by NLM denoising, which can improve the quality of EMD decomposition. To avoid modal aliasing problems and end effects, the signal is
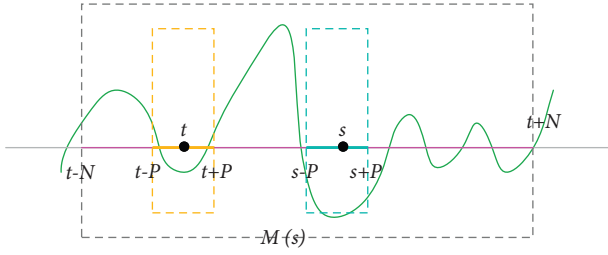
FIGURE 1: The relationship between the parameters of the NLM algorithm.
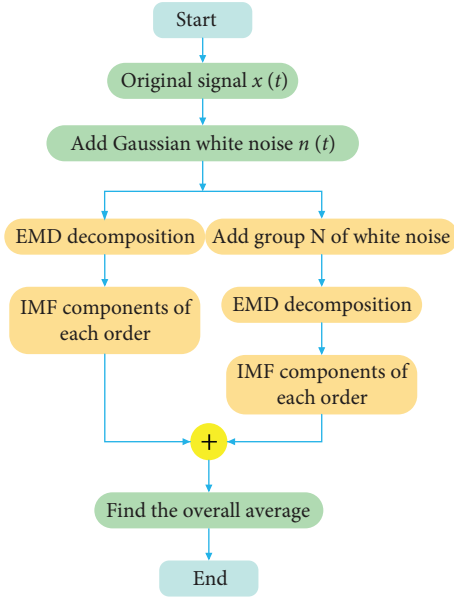

FIGURE 2: EEMD decomposition flow chart.

decomposed using the EEMD method. EEMD decomposes the signal into a set of IMF components with frequencies from high to low, removes some IMF components that do not meet the threshold condition, and adaptively reconstructs other remaining effective IMF components to obtain the final denoised signal.

Adaptive signal reconstruction [40, 41] is to select two evaluation indicators—correlation coefficient and root mean square error—that determine the effective IMF component by calculation and reconstructing the signal. The steps are as follows:

(1) The correlation coefficient between each IMF component and the original signal is calculated separately, and the calculation equation is as follows. In the equation, x represents the original signal, j represents the $j-th$ sampling point of the signal, and c_i represents the $i-th$ IMF component

decomposed $(i = 1, 2, \cdots, K)$; the larger the $Corr$, the higher the correlation.

$$Corr_i = \frac{\sum_{j=1}^{N}\left(x_j(j) - \overline{x(j)}\right)\left(c_i(j) - \overline{c_i(j)}\right)}{\sqrt{\sum_{j=1}^{N}\left(x(j) - \overline{x(j)}\right)^2 \sum_{j=1}^{N}\left(c_i(j) - \overline{c_i(j)}\right)^2}}. \quad (7)$$

(2) The root mean square error of each IMF component and the original signal is calculated separately, and the calculation equation is as follows. The smaller the RMSE, the closer it is to the original signal.

$$RMSE_i = \sqrt{\frac{\sum_{j=1}^{N}\left(x(j) - \overline{c_j(j)}\right)^2}{N}}. \quad (8)$$

(3) Calculating the adaptive threshold λ and δ, the equation is as follows. In the equation, K represents the number of IMF components, and the IMF components whose threshold satisfies the condition of Equation (10) are selected to reconstruct the signal.

$$\begin{cases} \lambda = \dfrac{\sum_{i=1}^{K-1} Corr_i}{K-1}, \\[2ex] \delta = \dfrac{\sum_{i=1}^{K-1} RMSE_i}{K-1} \\[2ex] \begin{cases} Corr_i \geq \lambda, \\[1ex] RMSE_i \leq \delta. \end{cases} \end{cases} \quad (9)$$

The flow chart of EEMD signal reconstruction is shown in Figure 3.

2.4. Simulation. The voice signal of the test library numbered FDAC1-SX304.WAV in the TIMIT standard library is selected, Gaussian white noise is added to make SNR = 0, the signal sampling frequency is set as 16000 Hz, and time-frequency domain analysis and NLM-EEMD noise reduction processing on the signal are performed. Time domain diagram, spectrogram, time spectrum, and Hilbert spectrum of the original signal are drawn in turn, as shown in Figure 4.

Adding Gaussian white noise to the original signal to make SNR = 0, and the original signal with noise is shown in Figure 5. The noisy original signal is first preprocessed by NLM, and the result is shown in Figure 6; then EEMD is
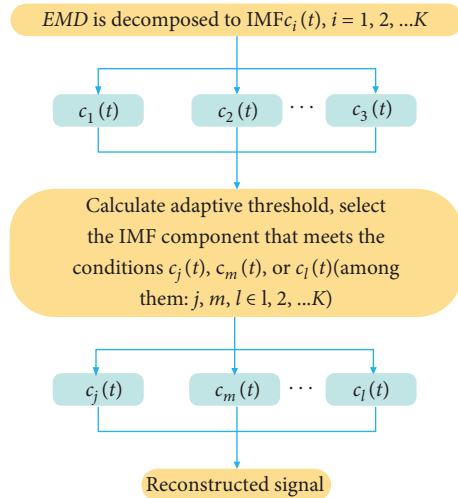
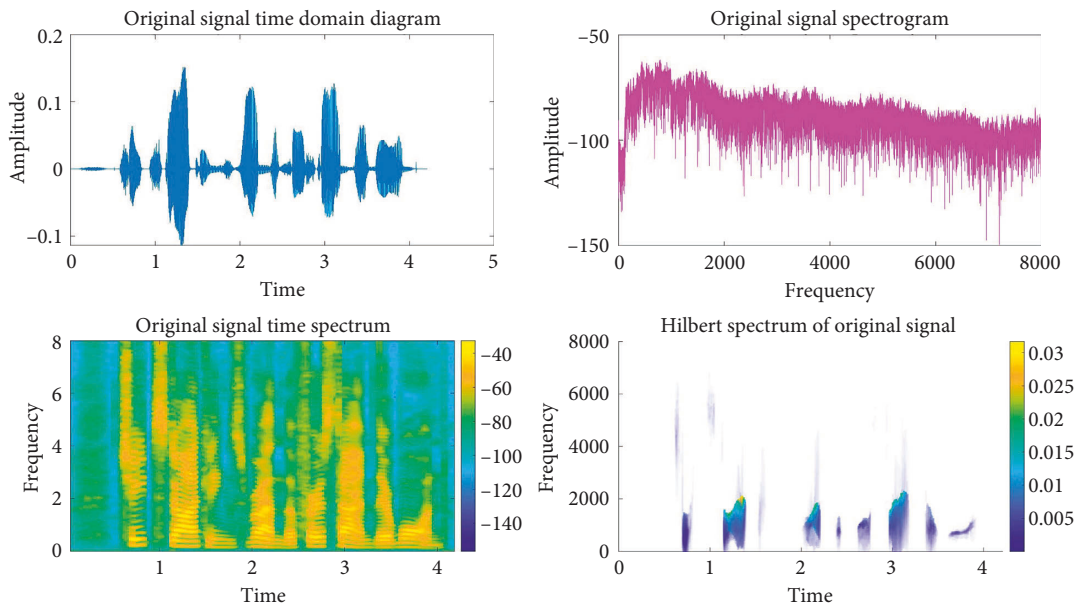Figure 3: Flow chart of EEMD reconstruction.

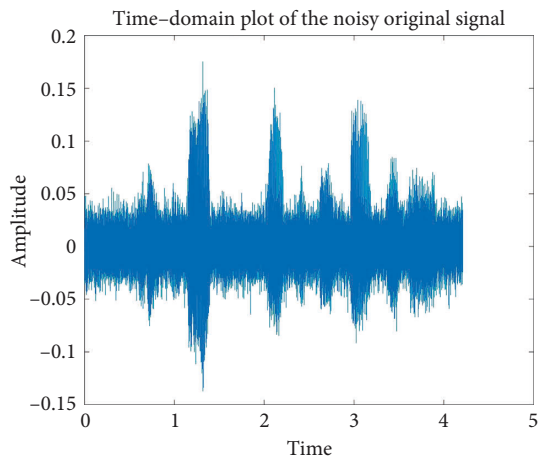Figure 4: Time-frequency analysis of the original signal.

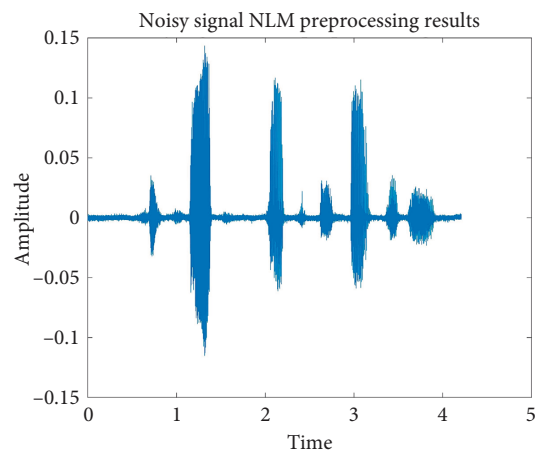Figure 5: Time domain diagram of the original signal with noise.

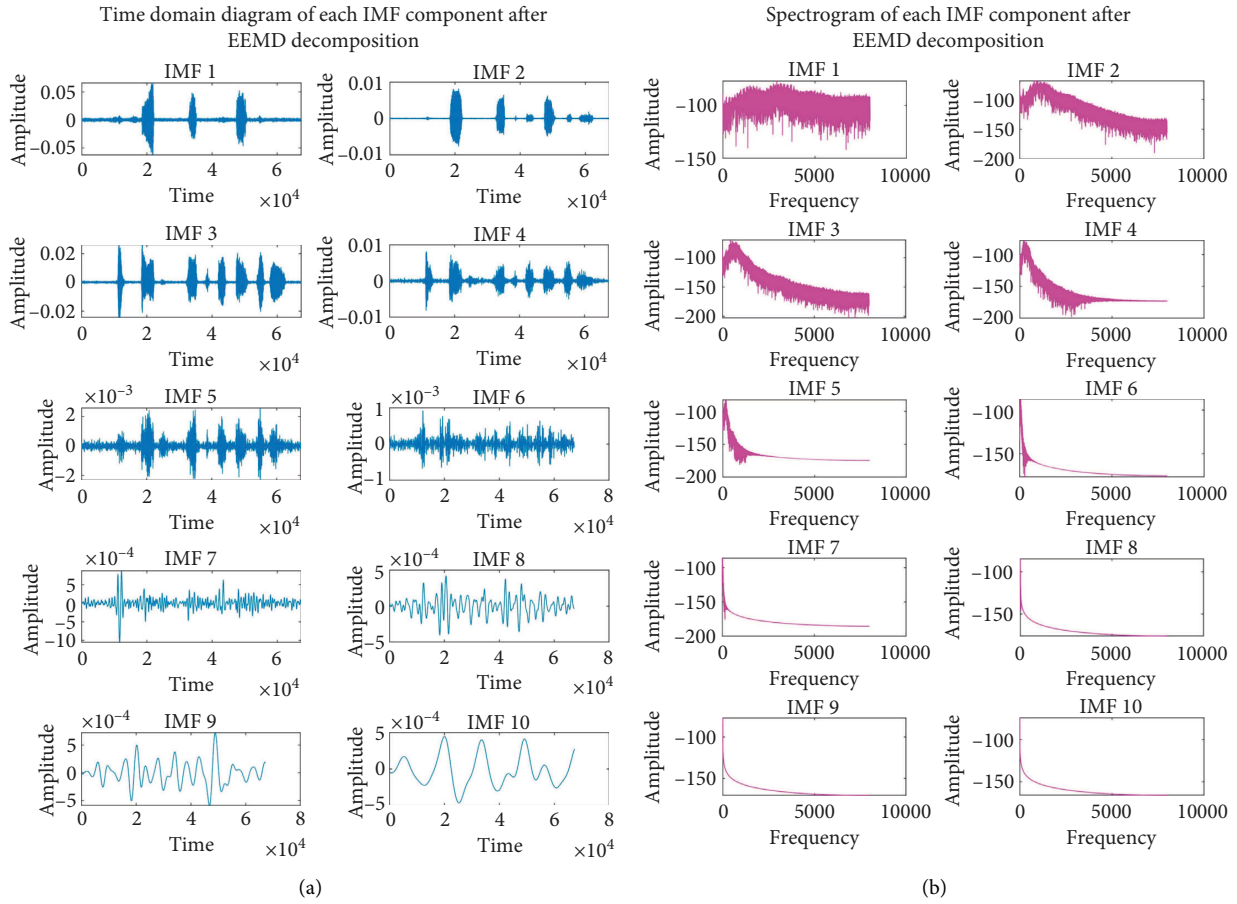Figure 6: NLM preprocessing result of noisy signal.

FIGURE 7: IMF components after EEMD decomposition. (a) Time domain diagram. (b) Spectrogram.

decomposed, and the decomposed IMF components and the remaining components and the corresponding spectrum are shown in Figure 7; the IMF components are distinguished according to frequency, it is divided into high-frequency component, low-frequency component, and trend quantity. The time domain diagram of each component is shown in Figure 8.

The correlation coefficient and root mean square error of each IMF component and residual component and the original signal are calculated, and then the adaptive threshold λ of 0.2692 and δ of 0.0074 are obtained. The IMF components with correlation coefficient greater than 0.2692 and root

mean square error less than 0.0074 are selected for reconstruction, and the adaptive reconstruction process is shown in Figures 9 and 10. According to the result of adaptive reconstruction, the components IMF1, IMF2, and IMF3 are selected for reconstruction. Figure 11 shows the comparison diagram of the signal before decomposition and the reconstructed signal and the reconstruction error diagram.

Figure 12 shows the comparison of original signal with the original signal with noise and the signal processed by NLM-EEMD; it can be seen that the denoising effect is very obvious, and the original signal characteristics are basically restored.
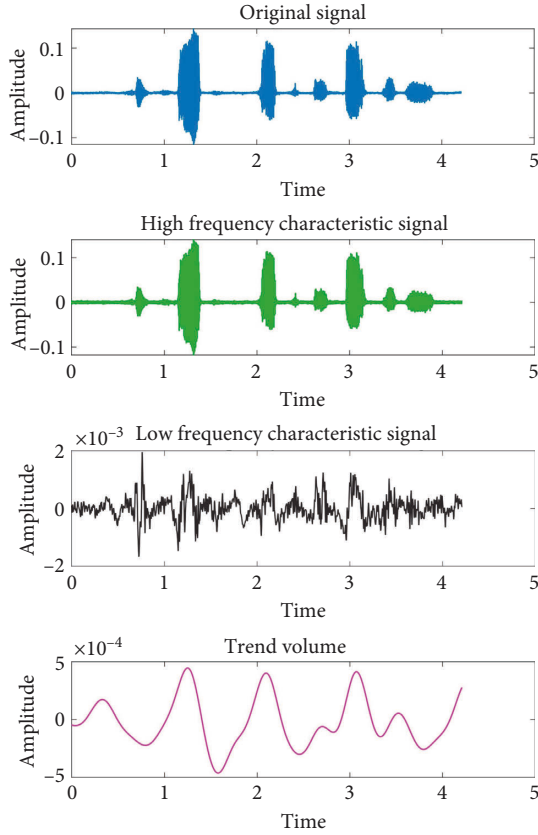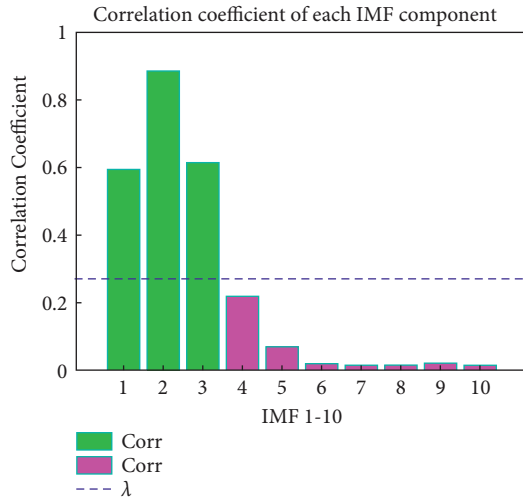
FIGURE 8: Frequency components of IMF components.

FIGURE 9: Correlation coefficient of each IMF component.

FIGURE 10: Root mean square error of each IMF component.
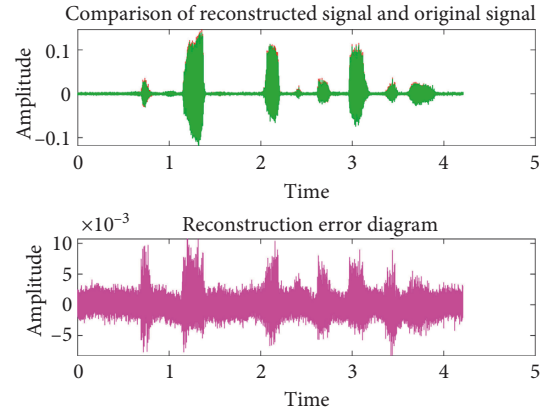
FIGURE 11: Comparison of reconstructed signal and original signal.

3. FCM-Generalized Quadratic Correlation Adaptive Delay Estimation Algorithm

3.1. FCM Algorithm. FCM algorithm (Fuzzy C-means algorithm) [22] is a clustering algorithm based on flexible fuzzy partition. This method uses the concept of determining the geometric closeness of data points in Euclidean space and obta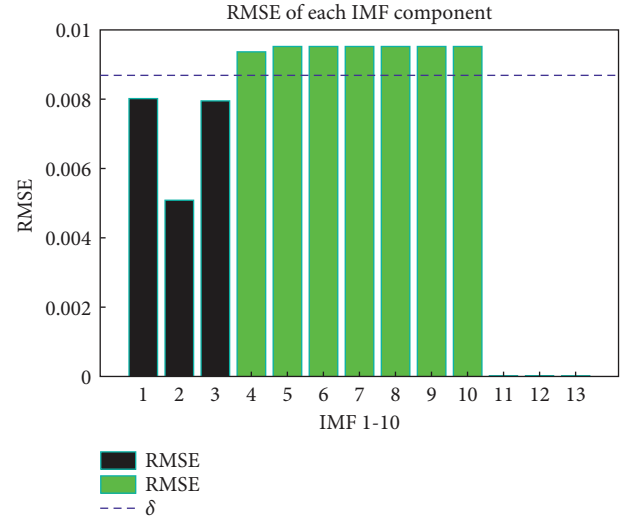ins the membership degree of each sample point to all class centers by optimizing the objective function, so as to automatically classify the samples.

Supposing the signal point sample is $X = \{x_1, x_2, \cdots x_n\}$, $c\,(2 \le c \le n)$ represents the number of cluster centers, $\{A_1, A_2, \cdots A_c\}$ represents the corresponding c categories, U represents fuzzy classification matrix, and $V = [v_1, v_2, \cdots v_n]$ represents the cluster center vector, we use the weighted sum of squared distances from the signal point X to each cluster center $v_i\,(1 \le i \le c)$ as the objective function:

$$J(U, V) = \sum_{j=1}^{n} \sum_{i=1}^{c} u_{ij}^m d_{ij}^2, \tag{10}$$

where m is the weighting parameter and u_{ij} and d_{ij} are the membership degree and Euclidean distance from the signal point sample x_j to the cluster center v_i, respectively.

The essence of the FCM algorithm is to repeatedly modify U and V through iteration. When the algorithm converges, theoretically, various cluster centers and the membership degrees of each sample to each pattern class are obtained, thus completing the fuzzy clustering division.
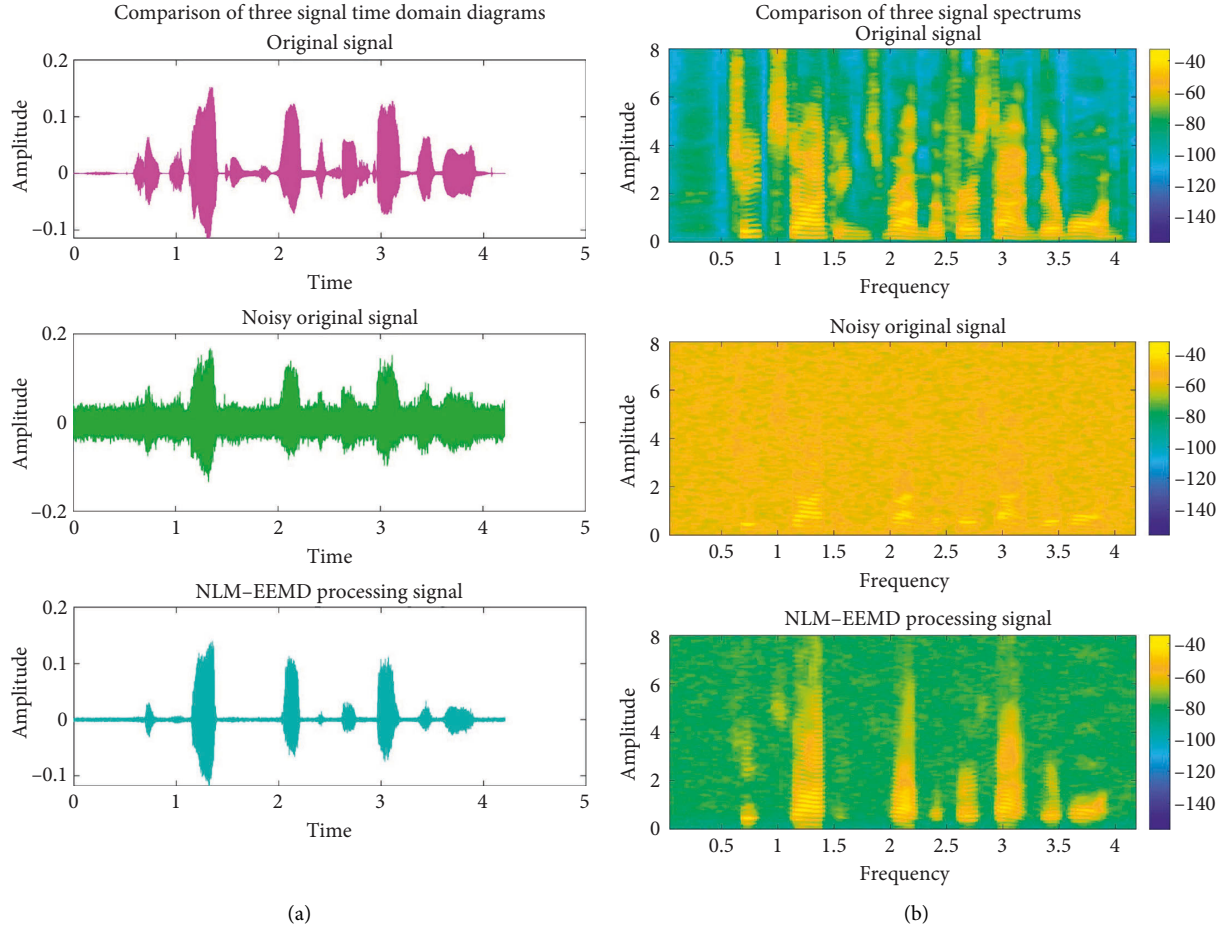
FIGURE 12: Comparison of original signal, noisy signal, and processed signal. (a) Time domain diagram. (b) Spectrogram.

3.2. Generalized Quadratic Correlation Delay Estimation Algorithm.

It is assumed that the acoustic signals collected by the two acoustic sensors are shown in Equation (11). In the equation, $s(n)$ represents the original sound source signal, α_1 and α_2 represent the attenuation factors of the two signals, $n_1(n)$ and $n_2(n)$ are noise, and τ represents the time delay difference between the sound source reaching the signals collected by the two sound sensors.

$$\begin{cases} x_1(n) = \alpha_1 s(n) + n_1(n) \\ x_2(n) = \alpha_2 s(n - \tau) + n_1(n) \end{cases}. \tag{11}$$

The simplest time delay estimation is to directly perform cross-correlation processing on the two signals $x_1(n)$ and $x_2(n)$, as shown in Equation (12).

$$R_{12}(\tau) = E[x_1(n)x_1(n - \tau)]. \tag{12}$$

Substituting (11) into Equation (13) to get:

$$\begin{aligned} R_{12}(\tau) = {} & \alpha_1\alpha_2 E[s(n - \tau_1)s(n - \tau_2 - \tau)] + \alpha_1 E[s(n - \tau_1)n_2(n - \tau)] \\ & + \alpha_2 E[s(n - \tau_2 - \tau)n_1(n)] + E[n_1(n)n_2(n - \tau)]. \end{aligned} \tag{13}$$

Because (n), $n_1(n)$, and $n_2(n)$ are not related to each other, (13) can be further simplified:

$$R_{12}(\tau) = \alpha_1\alpha_2 R_{ss}(\tau - \tau_{12}) + R_{n1n2}(\tau), \tag{14}$$

where $R_{ss}(\tau)$ represents the autocorrelation function of the sound source $s(n)$, and $R_{n1n2}(\tau)$ is the cross-correlation function of the two noises $n_1(n)$ and $n_2(n)$. If $n_1(n)$ and $n_2(n)$ are uncorrelated noises, (14) can be further simplified as: $R_{12}(\tau) = \alpha_1\alpha_2 R_{ss}(\tau - \tau_{12})$.

According to the properties of the correlation function, when $R_{12}(\tau)$ takes the maximum value, τ is the time delay difference between the sound source signal reaching the two acoustic sensors.

The generalized cross-correlation algorithm [42–44] transforms the cross-correlation function into the frequency domain and then weights the cross power spectrum to achieve the effect of suppressing noise, and then inversely transforms it to the time domain to obtain the generalized cross-correlation function. As shown in (15), $G_{x1x2}(\omega)$ refers to the cross power spectrum of the two collected signals, $\varphi_{12}(\omega)$ is the weighting function.

$$R_{12}(\tau) = \int_0^\pi \varphi_{12}(\omega)G_{x1x2}(\omega)e^{-j\omega\pi}d\omega. \tag{15}$$

Common weighting functions and their characteristics [45–49] are shown in Table 1.

TABLE 1: Common weighting functions and their characteristics.

| Name	Weighting function	Basic features
ROTH	$G_{x1x2}(\omega) = 1/G_{x1x1}(\omega)$	It is equivalent to Wiener filtering, which can effectively suppress areas with high noise power and error-prone signal estimation (i.e., areas with low signal-to-noise ratio) but will expand the peak of the cross-correlation function.
SCOT	$G_{x1x2}(\omega) = 1/\sqrt{G_{x1x1}(\omega)G_{x2x2}(\omega)}$	It is an improvement on ROTH weighting, considering the effects of both channels, but when $G_{x1x1}(\omega) = G_{x2x2}(\omega)$, SCOT is equivalent to ROTH, so it will also expand the peak of the cross-correlation function.
PHAT	$G_{x1x2}(\omega) = 1/|G_{x1x2}(\omega)|$	It is equivalent to whitening filtering, which has a better effect on large signal-to-noise ratios and is suitable for broadband signals. However, when $\hat{G}_{x1x2}(\omega) \neq G_{x1x2}(\omega)$, the correlation function is not a δ function; in addition, it is weighted by $G_{x1x2}(\omega)$. When the signal energy is small, the denominator approaches 0, thereby increasing the error. It can be improved by adding a fixed constant to the denominator.
Maximum likelihood weighting (ML)	$G_{x1x2}(\omega) = |\gamma(\omega)|^2/|G_{x1x2}(\omega)|(1 - |\gamma(\omega)|^2)$	$|\gamma(\omega)|^2$ is the modulo-squared coherence function, defined as $|\gamma(\omega)|^2 = |G_{x1x2}(\omega)|^2/G_{x1x1}(\omega)G_{x2x2}(\omega)$; the maximum likelihood weighting function gives a large weight to the frequency band with a large signal-to-noise ratio and a small weight to the frequency band of a small signal-to-noise ratio. In this way, the influence of noise can be better suppressed, and it is the optimal filter in the statistical sense.
HB weighted	$G_{x1x2}(\omega) = |G_{x1x2}(\omega)|/G_{x1x1}(\omega)G_{x2x2}(\omega)$	It has a suppressing effect on the periodic components in the signal, and the effect is similar to that of direct cross-correlation at low signal-to-noise ratio.
WP weighted	$G_{x1x2}(\omega) = |G_{x1x2}(\omega)|^2/G_{x1x1}(\omega)G_{x2x2}(\omega)$	When there are obvious periodic components in the signal, it fails; when the signal-to-noise ratio is low, the performance is not as good as PHAT.
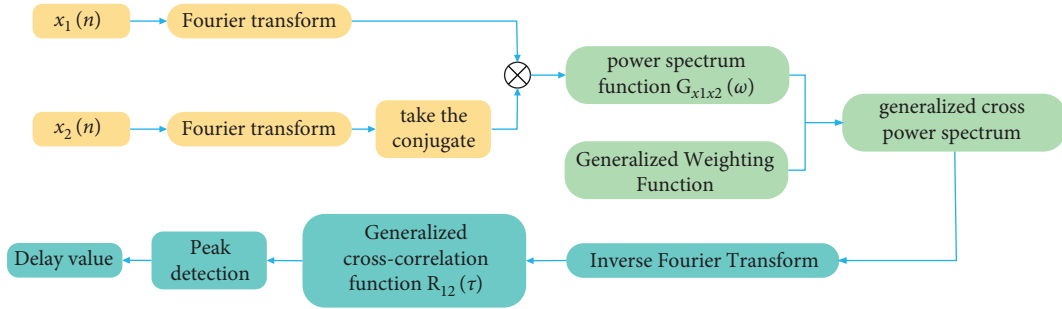
FIGURE 13: The principle block diagram of the generalized cross-correlation delay estimation algorithm.

The principle block diagram of the generalized cross-correlation delay estimation algorithm is shown in Figure 13.

The quadratic correlation algorithm [50–52] is also a common time delay estimation method. It performs a correlation operation on the autocorrelation function and the cross-correlation function of the two time domain signals to improve the time delay estimation accuracy.

$$
\begin{cases}
R_{11}(\tau) = E[x_1(n)x_1(n-\tau)] \\
R_{12}(\tau) = E[x_1(n)x_2(n-\tau)] \\
R_{RR}(\tau) = E[R_{11}(n)R_{12}(n-\tau)] \\
= E\begin{Bmatrix} [R_{ss}(n) + R_{sn1}(n) + R_{n1s}(n) + R_{n1n1}(n)] \\ [R_{ss}(n-D+\tau) + R_{n1s}(n-D+\tau) + R_{sn2}(n+\tau) + R_{n1n2}(n+\tau)] \end{Bmatrix}
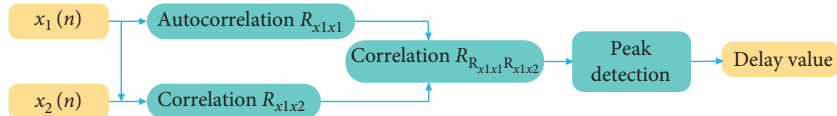\end{cases}
. \tag{16}
$$

Figure 14: The principle block diagram of quadratic correlation delay estimation.
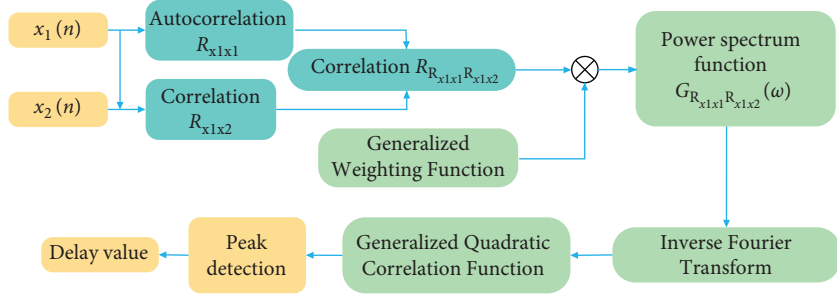

Figure 15: The principle block diagram of the generalized quadratic correlation delay estimation algorithm.
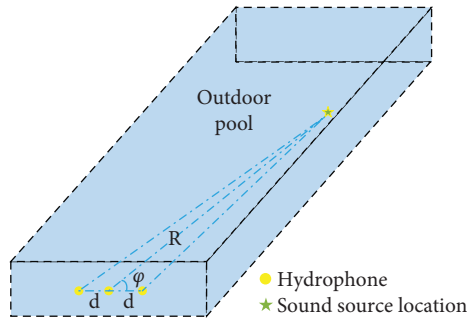
Figure 16: Schematic diagram of the experimental site.

Figure 17: Outdoor pool panorama.

Ignoring the cross-correlation function of signal and noise, (16) can be simplified as

$$R_{RR}(\tau) = R_{RS}(\tau - D) + R_{RN}(\tau), \qquad (17)$$

where R_{RS} represents pure signal for secondary correlation and R_{RN} represents noise for secondary autocorrelation. Compared with the primary correlation, the secondary correlation reduces the influence of noise on the signal and

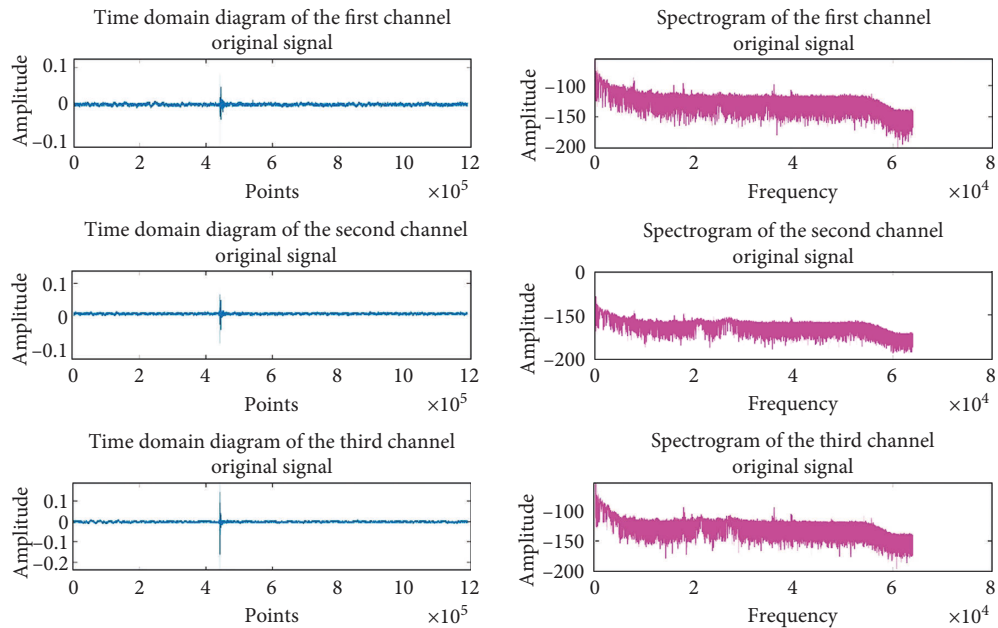FIGURE 18: Heavy object falling into water arouses water column diagram.

FIGURE 19: Time domain diagram and spectrum diagram of experimental signal.

can estimate the delay value more accurately in the low signal-to-noise ratio environment.

The block diagram of the quadratic correlation delay estimation is shown in Figure 14.

In this article, the advantages of generalized cross-correlation and quadratic correlation are combined for time delay estimation, that is, generalized quadratic correlation time delay estimation [50]. The principle block diagram is shown in Figure 15. The weighting function of generalized cross-correlation chooses SCOT weighting function.

3.3. Combination of Delay Estimation of FCM and Generalized Quadratic Correlation.
This article uses the FCM algorithm to adaptively extract the effective segment signal and then performs generalized quadratic

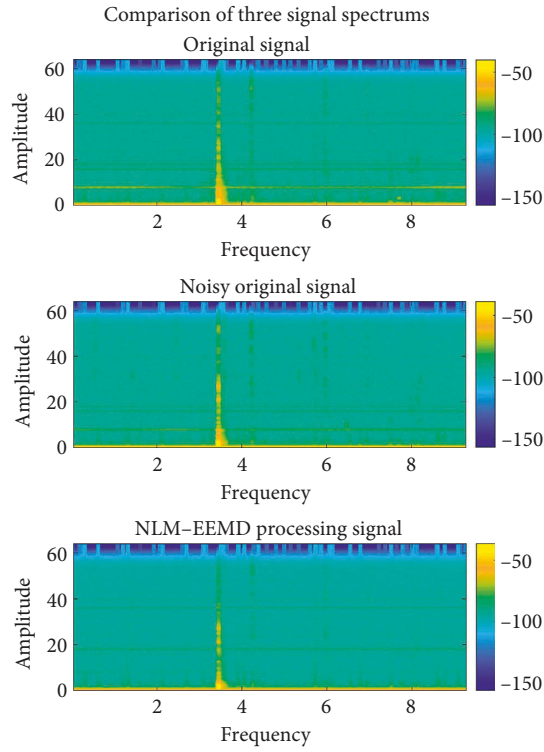Comparison of three signal spectrums

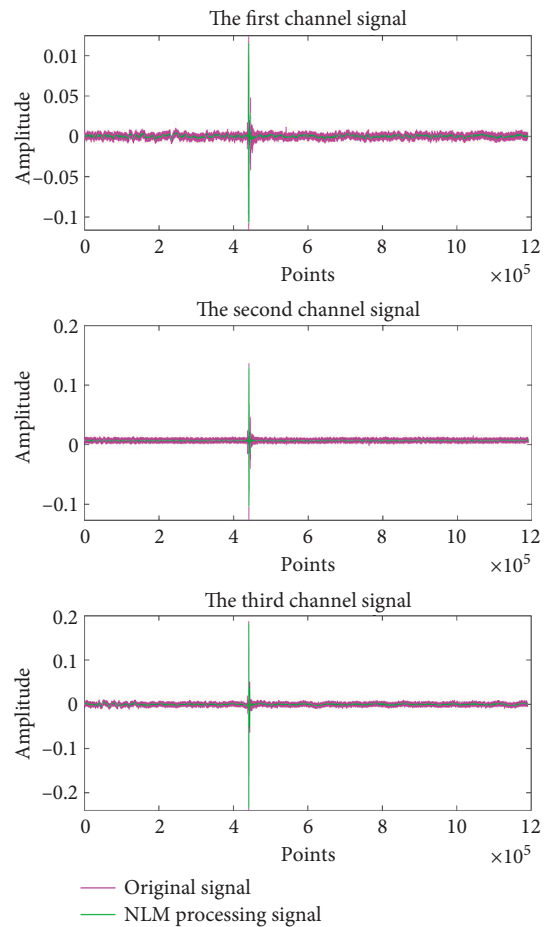FIGURE 20: Spectrum of experimental signal.

FIGURE 21: Comparison of the original value of the three-way signal and the NLM processing value.
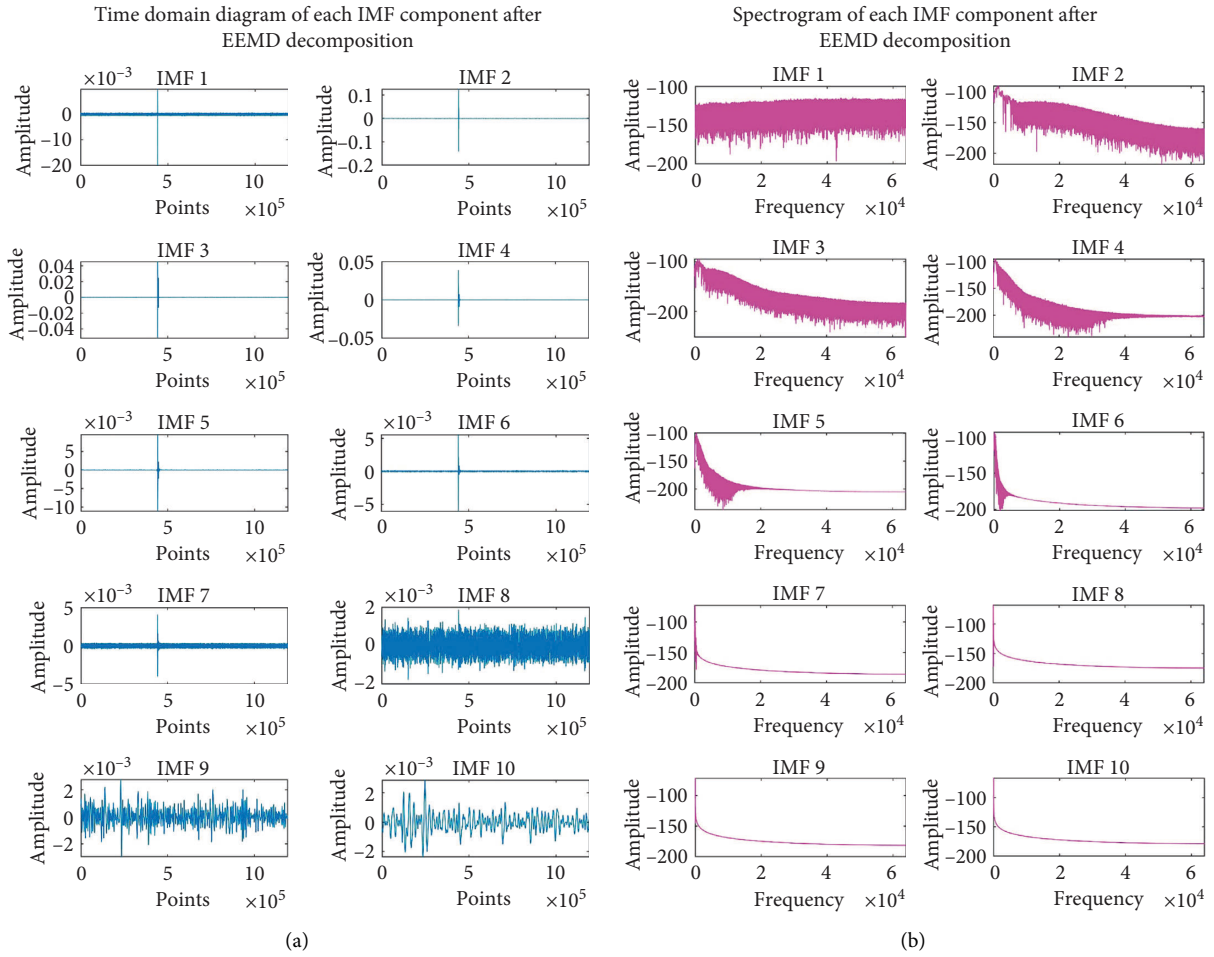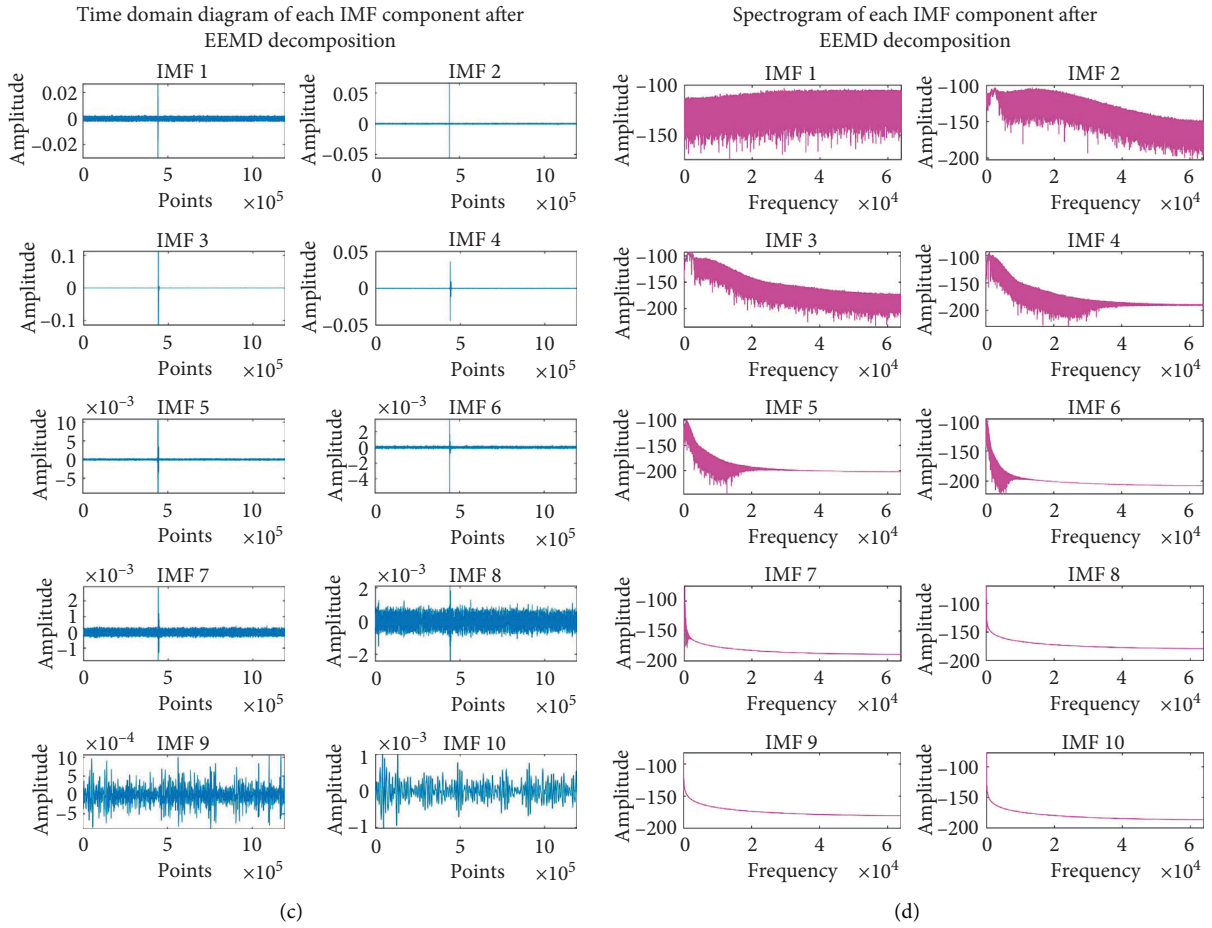
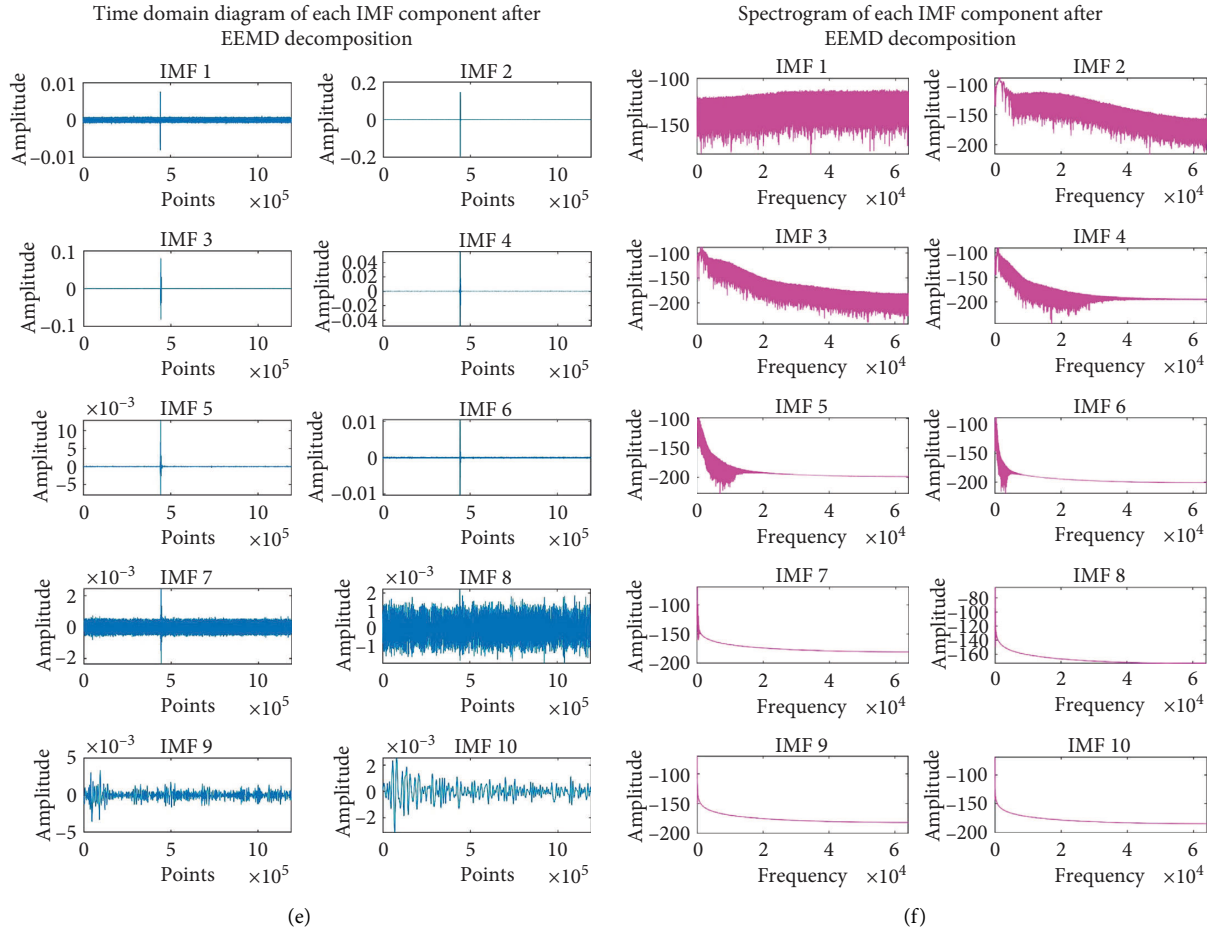FIGURE 22: Continued.

FIGURE 22: Continued.

(e)

(f)

Figure 22: Three-way signal EEMD decomposition. (a) Time domain diagram of the IMF component of the EMD decomposition of the first signal. (b) Spectrogram of the IMF component decomposed by EMD of the first signal. (c) Time domain diagram of the IMF component of the EMD decomposition of the second signal. (d) Spectrogram of the IMF component decomposed by EMD of the second signal. (e) Time domain diagram of the IMF component of the EMD decomposition of the third signal. (f) Spectrogram of the IMF component decomposed by EMD of the third signal.

correlation processing, which can sharpen the correlation peak and improve the accuracy of delay estimation. The steps are as follows [22]:

(1) In the FCM algorithm, the weighting parameter $m = 3$ is set, and the number of cluster centers is $c = 3$. The acoustic signal used for underwater positioning studied in this article is the shock signal, so it is divided into three categories: the front part of the shock signal, the shock signal generation segment, and the post-impact signal segment.

(2) Using FCM to process the acquired signal, the effective segment signal point samples are extracted and reconstructed, and the shock generation segment signal is obtained.

(3) For the acoustic signals received by other acoustic sensors, the same processing methods of steps (1) to (2) are adopted. In this way, each acoustic sensor corresponds to a signal of an impact generation segment, and the minimum value of the start point and the maximum value of the end point of these signals are taken as the final start point and end point, respectively, that is, the segment $\min(x(t_{start1}), x(t_{start2}), \cdots\cdots)$ to $\max(x(t_{end1}), x(t_{end2}), \cdots\cdots)$ is intercepted from the received signal of the acoustic sensor. The signal is processed as the final pending delay estimation.

(4) The generalized quadratic correlation delay estimation is performed to obtain the delay difference between the signals.

4. Experiment and Performance Analysis

4.1. The Principle and Process of Underwater Sound Source Localization. In this article, the ternary acoustic sensor array is used to collect the underwater sound source signal, and the time delay between the signal processing and the signal is estimated, and finally the underwater sound source
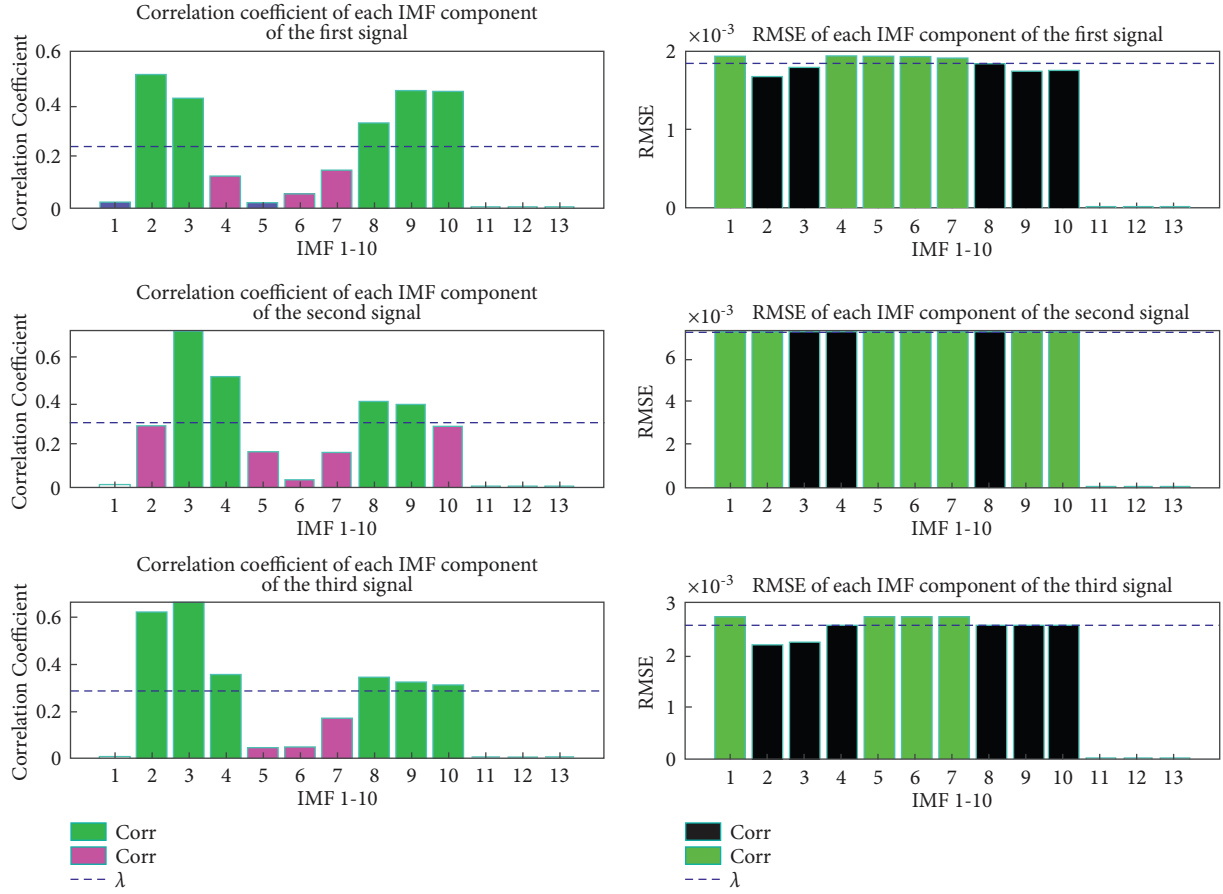
FIGURE 23: The process of adaptively selecting IMF components.

position is calculated by using the time delay difference. The schematic diagram of the experimental site is shown in Figure 16.

The azimuth distance equation used by the ternary acoustic sensor array for sound source localization is as follows:

$$\varphi = \cos^{-1}\left[\frac{cd^2\tau_{13} - c^3\tau_{12}\tau_{23}\tau_{13}}{2d^3 - c^2d\left(\tau_{12}^2 + \tau_{23}^2\right)}\right],$$

$$R = \frac{2d^2 - c^2\left(\tau_{12}^2 + \tau_{23}^2\right)}{2c\left(\tau_{12} - \tau_{23}\right)},$$

(18)

where φ is the azimuth of the explosion point to be estimated; $R_2 = R$ is the distance of the explosion point to be estimated; c is the speed of sound; d is the distance between the array elements; and τ_{12}, τ_{13}, and τ_{23} represent the time delay difference of the three-channel signals, respectively.

4.2. Experimental System Construction. The experimental device is built as shown in Figure 16, and the sound source localization experiment is conducted in a large outdoor pool. The underwater sound source signal is generated by throwing heavy objects at different angles and distances relative to the ternary array. The distance between the

elements of the ternary acoustic sensor array is 10 m and arranged in a straight line. The sensitivity of the acoustic sensor is less than −200 dB when detecting the sound source in the frequency range of 10 Hz–50000 Hz, the sampling frequency of the acquisition instrument is 128k Hz, and each acquisition time is set to 10 s (Figures 17 and 18).

4.3. Experimental Signal Processing. The collected acoustic signals at different locations are first analyzed in the time-frequency domain, and then NLM preprocessing, EEMD decomposition, and adaptive reconstruction are performed to obtain denoised signals. Finally, combined with the FCM algorithm, based on the generalized quadratic correlation delay estimation, the algorithm estimates the time delay of the three-channel signal in pairs and then solves the sound source position.

Taking the acoustic signal collected in an experiment as an example, the above analysis and processing are carried out. The time domain diagram and spectrogram and time spectrum of the signals collected by the three hydrophones are shown in Figures 19 and 20, respectively.

The comparison between the original signal of the three-channel signal and the NLM preprocessing results is shown in Figure 21, the NLM-EEMD denoising results are shown in Figure 22, and the signal adaptive reconstruction process is

Time domain diagram comparison of the first signal

The spectrum of the first NLM processing signal

Spectrum of the first reconstructed signal

——— NLM processing signal
——— Reconstructed signal

(a)

Time domain diagram comparison of the second signal

The spectrum of the second NLM processing signal

Spectrum of the second reconstructed signal

——— NLM processing signal
——— Reconstructed signal

(b)

FIGURE 24: Continued.

Time domain diagram comparison of the third signal

The spectrum of the third NLM processing signal

Spectrum of the third reconstructed signal

—— NLM processing signal
—— Reconstructed signal

(c)
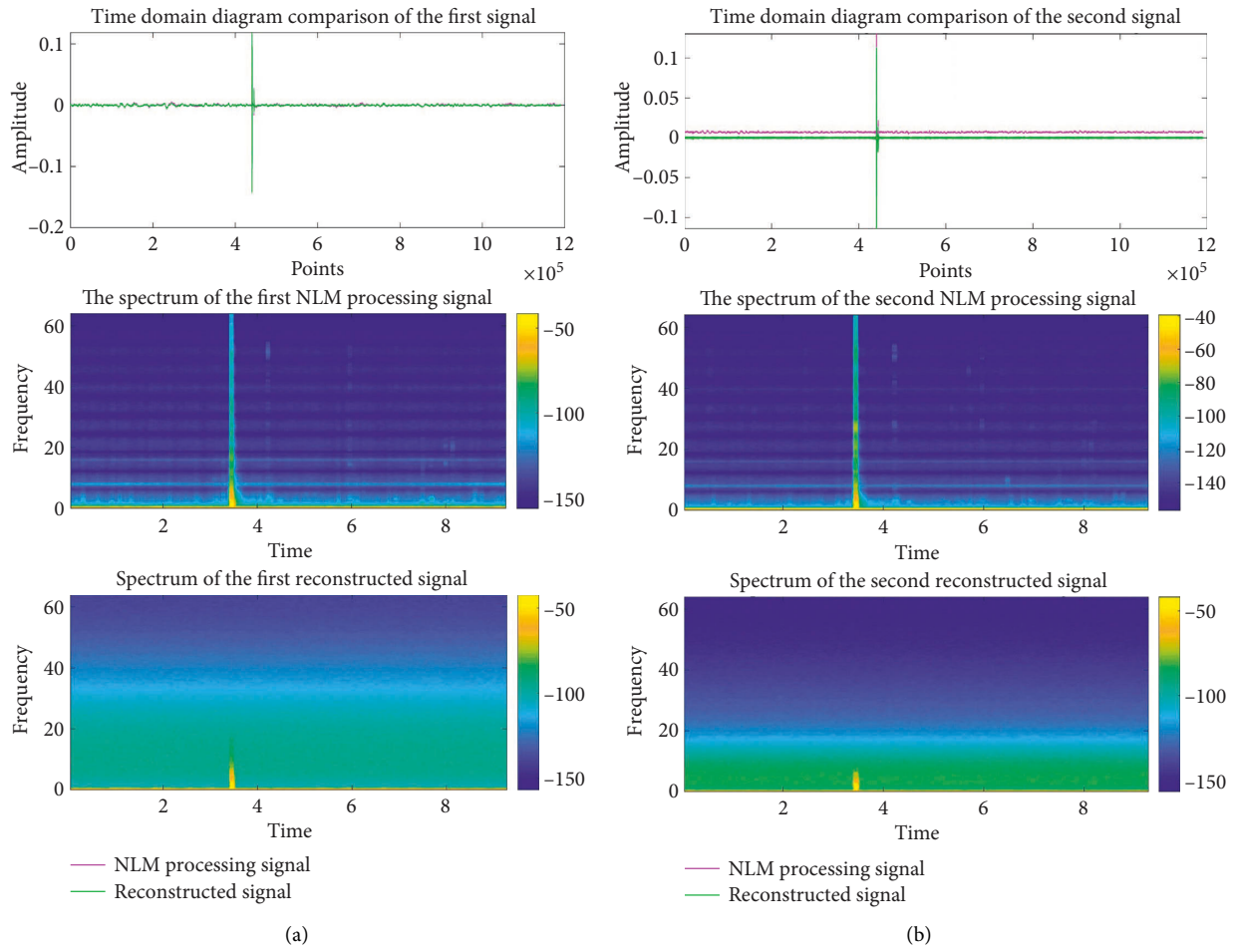
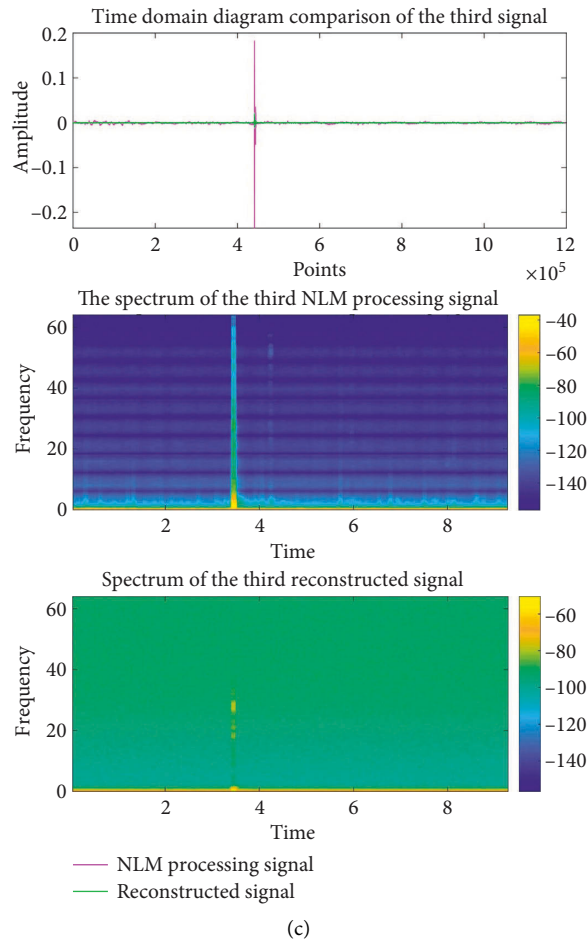Figure 24: Comparison of three-way NLM processing signal and reconstructed signal. (a) Comparison of the first NLM processing signal and the reconstructed signal. (b) Comparison of the second NLM processing signal and the reconstructed signal. (c) Comparison of the third NLM processing signal and the reconstructed signal.

The first channel signal reconstruction error

The second channel signal reconstruction error
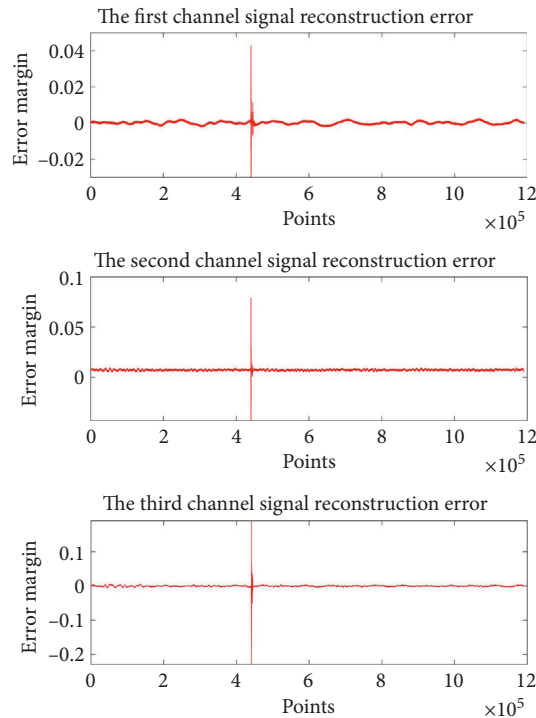
The third channel signal reconstruction error

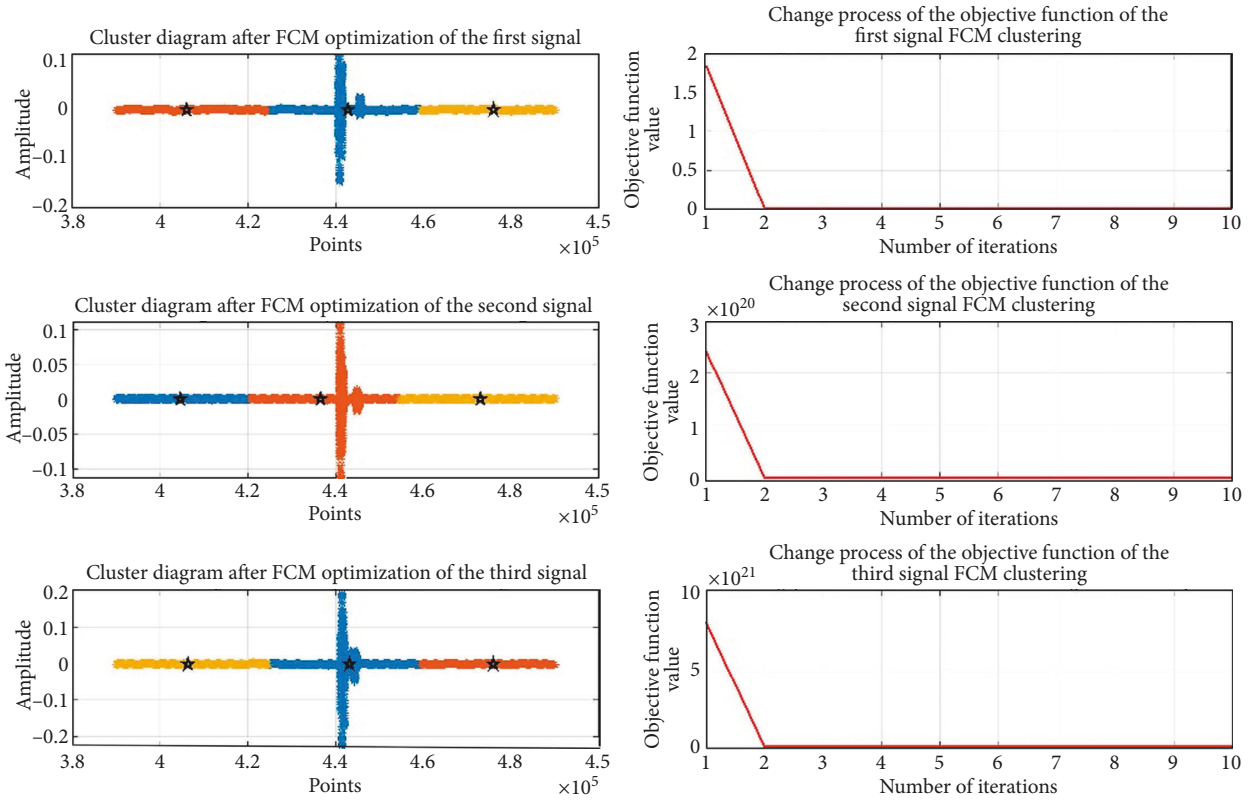Figure 25: Three-way signal reconstruction error.

FIGURE 26: The cluster diagram and objective function change process after three-channel signal FCM optimization.
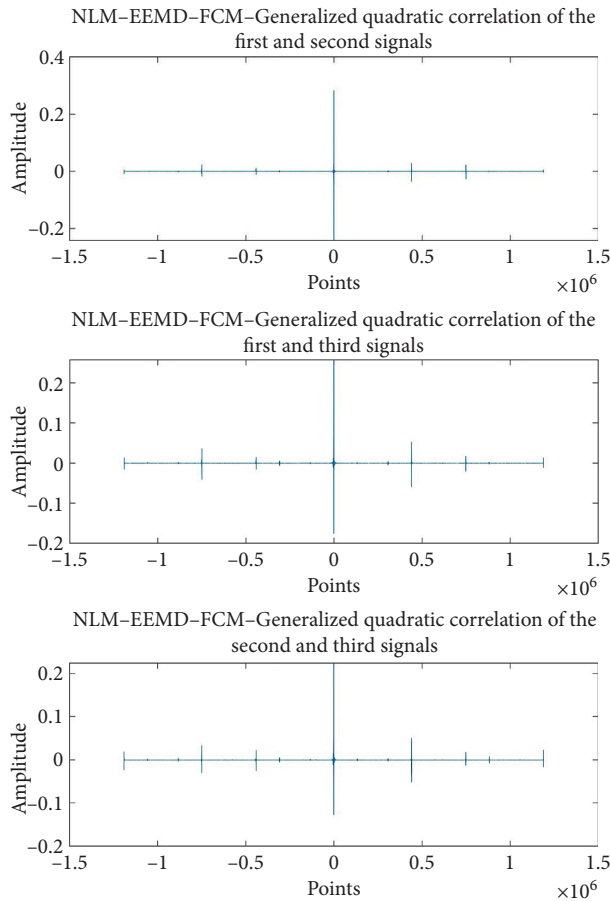

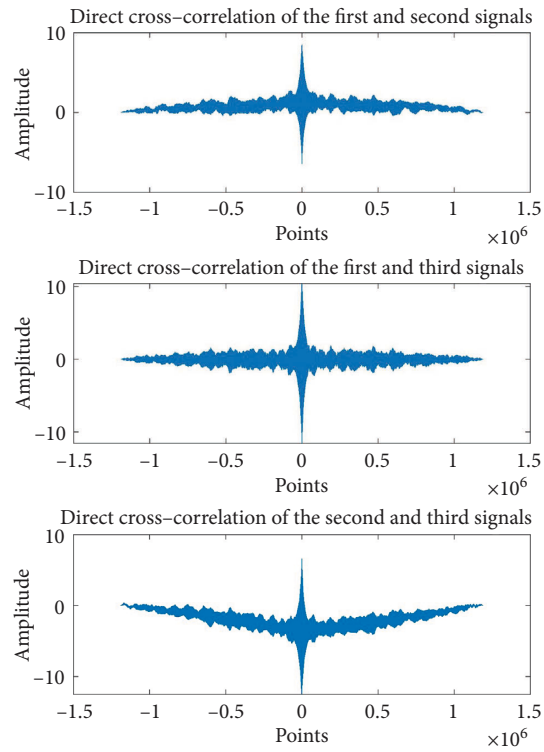FIGURE 27: NLM-EEMD-FCM-generalized quadratic correlation.
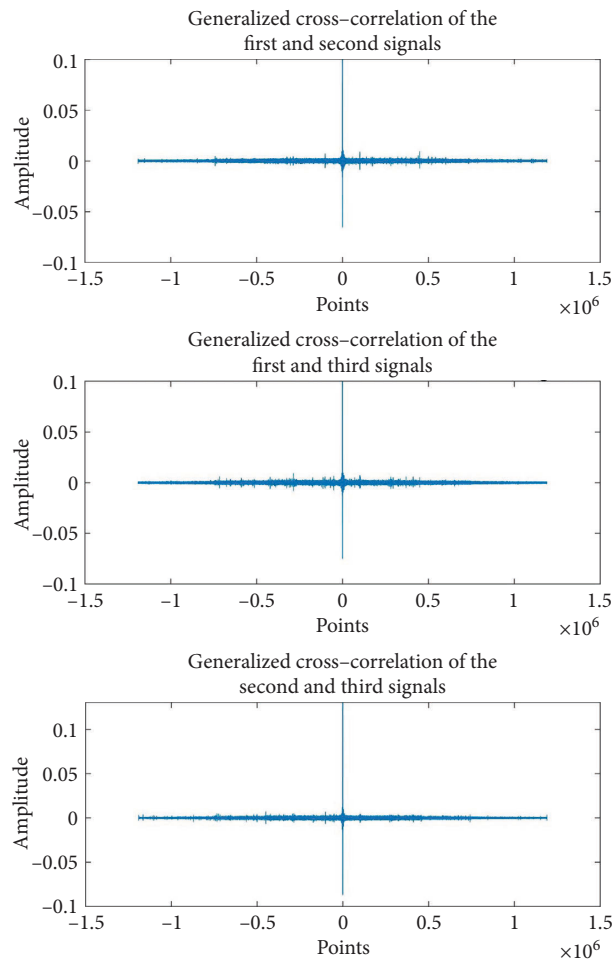
Figure 28: Direct cross-correlation.

Figure 29: Generalized cross-correlation.

Table 2: Comparison of positioning results of three delay estimation methods.

	Distance (m)	Azimuth (degrees)	Error (meters, degrees)
Theoretical calculation	85.1131	109.9209.	
Direct correlation	Invalid	Invalid	
Generalized cross-correlation	82.1087	110.7588	3.0044, 0.8379
NLM-EEMD-FCM-generalized quadratic correlation	83.5707	110.6450	1.5424, 0.7241

shown in Figure 23. The comparison between the reconstructed signal and the NLM processed signal is shown in Figure 24, and the reconstruction error is shown in Figure 25. It can be seen that the NLM preprocessing has an ideal de-drying effect. In the process of EEMD signal decomposition and reconstruction, the three signals are decomposed into 10 IMF components, adaptive threshold λ_1 is 0.2291, δ_1 is 0.0019, λ_2 is 0.2954, δ_2 is 0.0072, λ_3 is 0.2872, δ_3 is 0.0026, the first channel signal selects the 2nd, 3rd, 8th, 9th, and 10th components for reconstruction, the second channel signal selects the 3rd, 4th, and 8th components for reconstruction, the third channel signal selects the 2nd, 3rd, 4th, 8th, 9th, and 10th for reconstruction, and the original signal is basically restored, and the reconstruction error meets the requirements.

Figure 26 shows the clustering diagram and the change diagram of the clustering objective function after the three-channel signal is processed by FCM. Finally, the generalized quadratic correlation delay estimation is performed as shown in Figure 27.

4.4. Algorithm Verification and Analysis. In order to further verify the superiority of the algorithm in this article for underwater sound source localization, three different methods of direct cross-correlation method, generalized cross-correlation method, and generalized quadratic correlation method based on NLM-EEMD-FCM were used for the acoustic signals of the experiments in the previous section. The time delay estimation algorithm is used to calculate the sound source position. The delay estimation diagrams of direct cross-correlation and generalized cross-correlation are shown in Figures 28 and 29, respectively.

The positioning results of the three delay estimation methods are shown in Table 2.

It can be seen from Table 2 that the error is extremely large when using direct cross-correlation, which is basically invalid; for this group of collected signals, after the signal is processed by NLM-EEMD-FCM, the azimuth error is slightly improved, but compared with the distance error reduced by nearly 1.5 meters, it is negligible, so in general, the generalized quadratic correlation delay estimation method based on NLM-EEMD-FCM sharpens the peak value, improves the delay estimation accuracy, and reduces the underwater sound source localization error.

5. Conclusions

In order to improve the accuracy of underwater sound source location, an underwater sound source location method based on nonlocal mean overall average empirical mode decomposition (NLM-EEMD) autocorrelation denoising preprocessing and fuzzy C-means clustering (FCM)-generalized quadratic correlation time delay estimation is studied in this article. The experiment was carried out in a large outdoor pool. Through the analysis of the collected signal data, it was found that the NLM-EEMD adaptive denoising method has good effect, which improves the decomposition quality of EEMD. The FCM-generalized quadratic correlation method increases the correlation between two signals, sharpens the correlation peak, and improves the accuracy of time delay estimation. Taking the signal data analyzed above as an example, when the sound source distance is about 85 meters, the sound source location error based on NLM-EEMD and FCM-generalized quadratic correlation method is only 1.81%, which is 48.66% less than that of direct generalized cross-correlation method. This article provides a new idea to improve the accuracy of time delay estimation and also provides a certain reference for the research of high-precision positioning of underwater sound sources.

Data Availability

The data that support the findings of this study are available from the corresponding author upon reasonable request.

Conflicts of Interest

The authors declare that there are no conflicts of interest regarding the publication of this article.

Acknowledgments

References

[1] G. C. Carter, "Variance bounds for passively locating an acoustic source with a symmetric line array," *Journal of the Acoustical Society of America*, vol. 62, no. 4, pp. 922–926, 1977.

[2] J. H. DiBiase, "A high-accuracy, low-latency," *Technique for Talker Localization in Reverberant Environments Using Microphone arrays*, Brown University, Providence, RI, 2000.

[3] X. Wan and Z. Wu, "Improved steered response power method for sound source localization based on principal eigenvector," *Applied Acoustics*, vol. 71, no. 12, pp. 1126–1131, 2010.

[4] H. Do and H. F. Silverman, "A Fast Microphone Array SRP-PHAT Source Location Implementation Using Coarse-To-fine Region Contraction (CFRC)," in *Proceedings of the IEEE Workshop on Applications of Signal Processing to Audio and Acoustics*, pp. 295–298, IEEE, New Paltz, NY, USA, October 2007.

[5] M. V. S. Lima, W. A. Martins, L. O. Nunes et al., "A volumetric SRP with refinement step for sound source localization," *IEEE Signal Processing Letters*, vol. 22, no. 8, pp. 1098–1102, 2015.

[6] J. Tailiang, *Research on Speech Source Localization Methods Based on Microphone Arrays[J]*, University of Electronic Science and Technolgy of china, Si Chuan Sheng, China, 2006.

[7] T. Lobos, Z. Leonowicz, J. Rezmer, and P. Schegner, "High-resolution spectrum-estimation methods for signal analysis in power systems," *IEEE Transactions on Instrumentation and Measurement*, vol. 55, no. 1, pp. 219–225, 2006.

[8] M. Kaveh, "High resolution spectral estimation for noisy signals," *IEEE Transactions on Acoustics, Speech, & Signal Processing*, vol. 27, no. 3, pp. 286-287, 1979.

[9] T. H. Do, J. Hwang, and M. Yoo, "TDOA Based Indoor Visible Light Positioning systems," in *Proceedings of the Fifth International Conference on Ubiquitous and Future Networks (ICUFN)*, pp. 456–458, IEEE, Da Nang, Vietnam, July 2013.

[10] C. H. Knapp and G. C. Carter, "The generalized correlation method for estimation of time delay," *EEE Transactions on Acoustics, Speech, and Signal Processing*, vol. 24, no. 4, pp. 320–327, 1976.

[11] M. Omologo and P. Svaizer, "Acoustic event localization using a cross power spectrum phase based technique," in *Proceedings of IEEE International Conference on Acoustics, Speech, and Signal Processing*, pp. 273–276, Adelaide, SA, Australia, April 1994.

[12] L. Min, Z. Yumin, and Z. Ming, "A proposed time delay estimation in speech signal based on second correlation," *Journal of Applied Acoustics*, vol. 35, no. 3, pp. 255–264, 2016.

[13] P. Wang, X. T. Zhang, and L. Y. Xu, "Indoor near field ranging algorithm based on adaptive time delay estimation," *Chinese Journal of Computers*, vol. 40, pp. 1902–1917, 2017.

[14] S. Hwang, "Sound source localization using head-related transfer functions and weighted error function," *Acta Acustica united with Acustica*, vol. 105, no. 4, pp. 657–667, 2019.

[15] C. Fu-cheng, W. Shu-xun, and S. Xiao-ying, "High resolution and low complexity subspace based delay estimation for DS-UWB system," *Journal of Jilin University (Engineering and Technology Edition), China*, vol. 38, no. 2, pp. 471–475, 2008.

[16] S. Mosayyebpour, H. Lohrasbipeydeh, M. Esmaeili, and G. T. Aaron, "Time Delay Estimation via Minimum-phase and All-Pass Component processing," in *Proceedings of the IEEE International Conference on Acoustics, Speech and Signal Processing*, pp. 4285–4289, IEEE, Vancouver, BC, Canada, May 2013.

[17] Y. C. Heo, K. Kim, and Y. Lee, "Image denoising using non-local means (NLM) approach in magnetic resonance (mr) imaging: a systematic review," *Applied Sciences*, vol. 10, no. 20, p. 7028, 2020.

[18] M. Diwakar and M. Kumar, "CT image denoising using NLM and correlation-based wavelet packet thresholding," *IET Image Processing*, vol. 12, no. 5, pp. 708–715, 2018.

[19] S. Gaci, "A new ensemble empirical mode decomposition (EEMD) denoising method for seismic signals," *Energy Procedia*, vol. 97, pp. 84–91, 2016.

[20] T. Jin, Q. Li, and M. A. Mohamed, "A novel adaptive EEMD method for switchgear partial discharge signal denoising," *IEEE Access*, vol. 7, pp. 58139–58147, 2019.

[21] J. Jenitta and A. Rajeswari, "Denoising of ECG Signal Based on Improved Adaptive Filter with EMD and EEMD," in *Proceedings of the IEEE Conference on Information & Communication Technologies*, pp. 957–962, IEEE, Thuckalay, India, April 2013.

[22] J. Li, Y. Hou, S. Jin, and L. Dang, "Pipeline Leakage Location Based on NLM-EMD and FCM-Second correlation," *Application of Electronic Technique*, vol. 18, no. 11, 2018.

[23] S. Chen and D. Zhang, "Robust image segmentation using FCM with spatial constraints based on new kernel-induced distance measure," *IEEE Transactions on Systems, Man and Cybernetics, Part B (Cybernetics)*, vol. 34, no. 4, pp. 1907–1916, 2004.

[24] H. Sun, S. Wang, and Q. Jiang, "FCM-based model selection algorithms for determining the number of clusters," *Pattern Recognition*, vol. 37, no. 10, pp. 2027–2037, 2004.

[25] H. Zhong, C. Yang, and X. Zhang, "A new weight for nonlocal means denoising using method noise," *IEEE Signal Processing Letters*, vol. 19, no. 8, pp. 535–538, 2012.

[26] A. Rehman and Z. Wang, "SSIM-Based Non-local Means Image denoising," in *Proceedings of the 18th IEEE International Conference on Image Processing*, pp. 217–220, IEEE, Brussels, Belgium, September 2011.

[27] B. H. Tracey and E. L. Miller, "Nonlocal means denoising of ECG signals," *IEEE Transactions on Biomedical Engineering*, vol. 59, no. 9, pp. 2383–2386, 2012.

[28] Z. Li, L. Yu, J. D. Trzasko et al., "Adaptive nonlocal means filtering based on local noise level for CT denoising," *Medical Physics (Woodbury)*, vol. 41, no. 1, Article ID 011908, 2013.

[29] S. Kumar, D. Panigrahy, and P. K. Sahu, "Denoising of Electrocardiogram (ECG) signal by using empirical mode decomposition (EMD) with non-local mean (NLM) technique," *Biocybernetics and Biomedical Engineering*, vol. 38, no. 2, pp. 297–312, 2018.

[30] H. V. Bhujle and B. H. Vadavadagi, "NLM based magnetic resonance image denoising - a review," *Biomedical Signal Processing and Control*, vol. 47, pp. 252–261, 2019.

[31] M. Diwakar, P. Kumar, and A. K. Singh, "CT image denoising using NLM and its method noise thresholding," *Multimedia Tools and Applications*, vol. 79, no. 21-22, pp. 14449–14464, 2020.

[32] J. Froment, "Parameter-free fast pixelwise non-local means denoising," *Image Processing On Line*, vol. 4, pp. 300–326, 2014.

[33] Y. Li, B. Tang, and Y. Yi, "A novel complexity-based mode feature representation for feature extraction of ship-radiated noise using VMD and slope entropy," *Applied Acoustics*, vol. 196, Article ID 108899, 2022.

[34] Y. Li, B. Tang, X. Jiang, and Y. Yi, "Bearing fault feature extraction method based on GA-VMD and center frequency," *Mathematical Problems in Engineering*, vol. 2022, pp. 1–19, 2022.

[35] G. Singh, G. Kaur, and V. Kumar, "ECG Denoising Using Adaptive Selection of IMFs through EMD and EEMD," in *Proceedings of the International Conference on Data Science & Engineering (ICDSE)*, pp. 228–231, IEEE, Kochi, India, August 2014.

[36] Y. Jia, G. Li, X. Dong, and K. He, "A novel denoising method for vibration signal of hob spindle based on EEMD and grey theory," *Measurement*, vol. 169, Article ID 108490, 2021.

[37] K. Kærgaard, S. H. Jensen, and S. Puthusserypady, "A comprehensive performance analysis of EEMD-BLMS and DWT-NN hybrid algorithms for ECG denoising[J]," *Biomedical Signal Processing and Control*, vol. 25, pp. 178–187, 2016.

[38] G. Liu and Y. Luan, "An adaptive integrated algorithm for noninvasive fetal ECG separation and noise reduction based on ICA-EEMD-WS," *Medical, & Biological Engineering & Computing*, vol. 53, no. 11, pp. 1113–1127, 2015.

[39] Y. Zhang, J. Lian, and F. Liu, "An improved filtering method based on EEMD and wavelet-threshold for modal parameter identification of hydraulic structure," *Mechanical Systems and Signal Processing*, vol. 68-69, pp. 316–329, 2016.

[40] M. Yang, X. Chen, J. Du, and Y. Cui, "Ultra-short-term multistep wind power prediction based on improved EMD and reconstruction method using run-length Analysis," *IEEE Access*, vol. 6, pp. 31908–31917, 2018.

[41] C. Guo, Y. Chen, J. Yuan, Y. Zhu, Q. Cheng, and X. Wang, "Biomedical photoacoustic imaging optimization with deconvolution and EMD reconstruction," *Applied Sciences*, vol. 8, no. 11, p. 2113, 2018.

[42] M. Azaria and D. Hertz, "Time delay estimation by generalized cross correlation methods," *IEEE Transactions on Acoustics, Speech, & Signal Processing*, vol. 32, no. 2, pp. 280–285, 1984.

[43] L. Chen, Y. Liu, F. Kong, and N He, "Acoustic source localization based on generalized cross-correlation time-delay estimation," *Procedia Engineering*, vol. 15, pp. 4912–4919, 2011.

[44] N. Quaegebeur, T. Padois, P. A. Gauthier, and P Masson, "Enhancement of time-domain acoustic imaging based on generalized cross-correlation and spatial weighting," *Mechanical Systems and Signal Processing*, vol. 75, pp. 515–524, 2016.

[45] B. Van Den Broeck, A. Bertrand, and P. Karsmakers, "Time-domain Generalized Cross Correlation Phase Transform Sound Source Localization for Small Microphone arrays," in *Proceedings of the 5th European DSP Education and Research Conference (EDERC)*, pp. 76–80, IEEE, Amsterdam, Netherlands, September 2012.

[46] Y. Wang, P. Li, J. Zhang et al., "Distributed optical fiber vibration sensor using generalized cross-correlation algorithm," *Measurement*, vol. 144, pp. 58–66, 2019.

[47] J. M. Villladangos, J. Ureña, J. J. García et al., "Measuring time-of-flight in an ultrasonic LPS system using generalized cross-correlation," *Sensors*, vol. 11, no. 11, pp. 10326–10342, 2011.

[48] T. Padois, O. Doutres, and F. Sgard, "On the use of modified phase transform weighting functions for acoustic imaging with the generalized cross correlation," *Journal of the Acoustical Society of America*, vol. 145, no. 3, pp. 1546–1555, 2019.

[49] T. Padois, "Acoustic source localization based on the generalized cross-correlation and the generalized mean with few microphones," *Journal of the Acoustical Society of America*, vol. 143, no. 5, pp. EL393–EL398, 2018.

[50] A. Mahalanobis, R. R. Muise, S. R. Stanfill, and A. Van Nevel, "Design and application of quadratic correlation filters for target detection," *IEEE Transactions on Aerospace and Electronic Systems*, vol. 40, no. 3, pp. 837–850, 2004.

[51] A. Mahalanobis, R. R. Muise, and S. R. Stanfill, "Quadratic correlation filter design methodology for target detection and surveillance applications," *Applied Optics*, vol. 43, no. 27, pp. 5198–5205, 2004.

[52] J. A. Pople, M. Head-Gordon, and K. Raghavachari, "Quadratic configuration interaction. A general technique for determining electron correlation energies," *Journal of Chemical Physics*, vol. 87, no. 10, pp. 5968–5975, 1987.